ARTICLE

Modeling disease trajectory in Duchenne muscular dystrophy

William D. Rooney, PhD, Yosef A. Berlow, MD, PhD, William T. Triplett, MS, Sean C. Forbes, PhD, Rebecca J. Willcocks, PhD, Dah-Jyuu Wang, PhD, Ishu Arpan, PhD, Harneet Arora, PT, PhD, Claudia Senesac, PT, PhD, Donovan J. Lott, PT, PhD, Gihan Tennekoon, MBBS, Richard Finkel, MD, Barry S. Russman, MD, Erika L. Finanger, MD, Saptarshi Chakraborty, PhD, Elliott O'Brien, MS, Brendan Moloney, MS, Alison Barnard, DPT, PhD, H. Lee Sweeney, PhD, Michael J. Daniels, ScD, Glenn A. Walter, PhD, and Krista Vandenborne, PhD

Correspondence
Dr. Rooney
rooneyw@ohsu.edu

Neurology® 2020;94:e1622-1633. doi:10.1212/WNL.0000000000009244

Abstract

Objective

To quantify disease progression in individuals with Duchenne muscular dystrophy (DMD) using magnetic resonance biomarkers of leg muscles.

Methods

MRI and magnetic resonance spectroscopy (MRS) biomarkers were acquired from 104 participants with DMD and 51 healthy controls using a prospective observational study design with patients with DMD followed up yearly for up to 6 years. Fat fractions (FFs) in vastus lateralis and soleus muscles were determined with ^{1}H MRS. MRI quantitative T_2 (qT_2) values were measured for 3 muscles of the upper leg and 5 muscles of the lower leg. Longitudinal changes in biomarkers were modeled with a cumulative distribution function using a nonlinear mixed-effects approach.

Results

MRS FF and MRI qT_2 increased with DMD disease duration, with the progression time constants differing markedly between individuals and across muscles. The average age at half-maximal muscle involvement (μ) occurred 4.8 years earlier in vastus lateralis than soleus, and these measures were strongly associated with loss-of-ambulation age. Corticosteroid treatment was found to delay μ by 2.5 years on average across muscles, although there were marked differences between muscles with more slowly progressing muscles showing larger delay.

Conclusions

MRS FF and MRI qT_2 provide sensitive noninvasive measures of DMD progression. Modeling changes in these biomarkers across multiple muscles can be used to detect and monitor the therapeutic effects of corticosteroids on disease progression and to provide prognostic information on functional outcomes. This modeling approach provides a method to transform these MRI biomarkers into well-understood metrics, allowing concise summaries of DMD disease progression at individual and population levels.

ClinicalTrials.gov identifier:

NCT01484678.

From the Advanced Imaging Research Center (W.D.R., Y.A.B., I.A., E.O., B.M.), Department of Neurology (W.D.R., I.A., B.S.R., E.L.F.), Department of Biomedical Engineering (W.D.R.), Department of Behavioral Neuroscience (W.D.R., Y.A.B.), and Department of Pediatrics (B.S.R., E.L.F.), Oregon Health & Science University, Portland; Departments of Physical Therapy (W.T.T., S.C.F., R.J.W., H.A., C.S., D.J.L., K.V.), Statistics (S.C., M.J.D.), Physiology and Functional Genomics (A.B., G.A.W.), and Pharmacology & Therapeutics (H.L.S.), University of Florida, Gainesville; Department of Radiology (D.-J.W.) and Division of Neurology (G.T.), Children's Hospital of Philadelphia, PA; Department of Pediatrics (R.F.), Nemours Children's Hospital, Orlando, FL; and Shriners Hospital (B.S.R., E.L.F.), Portland, OR.

Go to Neurology.org/N for full disclosures. Funding information and disclosures deemed relevant by the authors, if any, are provided at the end of the article.

Glossary

BFLH = biceps femoris long head; **CDF** = cumulative distribution function; **CHOP** = Children's Hospital of Philadelphia; **DMD** = Duchenne muscular dystrophy; **FF** = fat fraction; **GRA** = gracilis; **HR** = hazard ratio; **LOA** = loss of ambulation; **MG** = medial gastrocnemius; **MR** = magnetic resonance; **MRS** = magnetic resonance spectroscopy; **MSME** = multislice multispin echo; **NLME** = nonlinear mixed-effect; **OHSU** = Oregon Health & Science University; **PER** = peroneus; **qT_2** = quantitative T_2; **SOL** = soleus; **TA** = tibialis anterior; **TE** = echo time; **TP** = tibialis posterior; **TR** = repetition time; **UF** = University of Florida; **VL** = vastus lateralis.

Duchenne muscular dystrophy (DMD) is a progressive neuromuscular disease caused by the absence of functional dystrophin in muscles.[1–3] Skeletal muscles in DMD are characterized by sarcolemmal fragility, inflammation, myofiber breakdown and regeneration, and ultimately replacement of contractile tissue with fatty infiltrate and concomitant tissue fibrosis.[3,4] Currently, there is no cure for DMD,[5–7] but several promising therapies have been identified, with some currently being evaluated in clinical trials and others at various stages in the clinical pipeline.[8] To more quickly evaluate new DMD therapies, there is a pressing need for improved biomarkers that are sensitive to disease progression and can readily be deployed at multiple sites.[9–11]

MRI and magnetic resonance (MR) spectroscopy (MRS) offer a significant promise in this regard.[10,12] These noninvasive, widely available techniques offer excellent sensitivity for the detection of DMD muscle pathology.[13,14] In addition, we need a more complete and systematic understanding of the natural history of skeletal muscle disease progression compiled from a large DMD cohort to better appreciate progression heterogeneity and to provide an improved context to evaluate new therapies. Here, we present a comprehensive characterization of the natural disease progression in DMD by modeling longitudinal changes in quantitative MR biomarkers from lower limb muscles in the ImagingDMD cohort.

Our primary goal was to quantify DMD disease progression using MR biomarkers in combination with a simple and accessible modeling approach. The modeling approach was investigated in the context of well-characterized features of DMD disease progression, including spatiotemporal aspects of leg muscle involvement, relationship of muscle involvement to loss of ambulation (LOA), and impact of corticosteroid treatment on measures of disease progression.

Methods

Participants and study design

The data were collected as part of a multicenter study, ImagingDMD (imagingdmd.org/), a prospective observational study of DMD to characterize the natural history of leg muscle involvement, conducted at the University of Florida (UF), Oregon Health & Science University (OHSU), and Children's Hospital of Philadelphia (CHOP). Our team enrolled 174 individuals with DMD and 51 healthy male controls between September 2011 and May 2018. Details of eligibility criteria and sources and methods of recruitment are provided in our previous publications.[9,15,16] Briefly, a team member at each site obtained a detailed medical history from the participants, and the diagnosis of DMD was confirmed on the basis of (1) clinical features with onset of symptoms before 5 years of age, (2) elevated serum creatine kinase, and (3) absence of dystrophin expression, as determined by immunostaining or Western blot (<2%), and/or DNA confirmation of a dystrophin mutation.

For this natural history disease progression study, we excluded individuals with DMD who participated in clinical trials, leaving 104 individuals with DMD and 51 healthy controls for analysis. Subjects with DMD were followed up for up to 6 years, with a primary follow-up interval of 12 months. Subject accrual occurred on a rolling basis, which resulted in participants being studied for variable amounts of time. The following is a summary of DMD participant numbers at each time point (fraction of baseline): baseline n = 104 (1.00), ≥1 year n = 85 (0.82), ≥2 years n = 65 (0.62), ≥3 years n = 56 (0.54), ≥4 years n = 50 (0.48), ≥5 years n = 38 (0.37), and ≥6 years n = 20 (0.19). Finally, a subset of participants with DMD (n = 12) were studied at shorter intervals (at 3- and 6-month intervals after the baseline visit) to evaluate the effects of transitioning to corticosteroid treatment. Those results have been described.[16]

Standard protocol approvals, registrations, and patient consents

The Institutional Review Boards at the 3 institutions (UF, OHSU, and CHOP) approved the study, and the study was registered on ClinicalTrials.gov (NCT01484678). A parent/guardian provided informed written consent, and each participant provided written assent before study participation.

MRI/MRS acquisition

All MRI/MRS data were acquired by trained operators using standardized procedures detailed in a manual of operating procedures using whole-body 3T MRI instruments located at 3 institutions: (1) site 1 (UF), Philips (Best, the Netherlands) Achieva 3T whole-body imaging system with a transmit/receive phased-array knee radiofrequency coils (InVivo) for lower leg, and a 2 or 8-channel surface coil receive with body coil transmit for the upper leg; (2) site 2 (OSHU), Siemens (Malvern, PA) TIM Trio 3T (later Prisma) instrument using an extremity quadrature transmit/receive radiofrequency coil for lower and upper leg, and (3) site 3 (CHOP), Siemens

Verio TIM 3T instrument using a body radiofrequency coil transmit and receive only 8-channel array coil for the lower leg and a 4-channel flex receive coil for the upper leg. All participants were advised to avoid extensive physical activity for 3 days before MRI/MRS study visits. The total time required to complete the MR acquisition for the lower and upper leg was 1 to 1.5 hours. Trained/certified team members analyzed MRI/MRS data at a central site (UF) using automated processing procedures whenever possible. Finally, all data were reviewed critically by the MR working group during biweekly web conferences to ensure consistent quality throughout the study.

We acquired proton (^{1}H) MRS data to measure fat fraction (FF) using a water nonsuppressed Stimulated Echo Acquisition Mode[17,18] (echo time [TE] 108 milliseconds, repetition time [TR] 3,000 milliseconds, 64 averages) single-voxel approach applied in the vastus lateralis (VL) and soleus (SOL) muscles of the right leg, requiring 3 minutes total acquisition time for each muscle. The voxel position was selected in the belly of the muscle, and its size was adjusted to maximize the volume of interest of each muscle while avoiding contamination from the fascia and other muscle groups.[9] The operators ensured that the voxel size and position were matched with the baseline to be consistent for all follow-up visits.

Axial images of the lower and upper right leg were acquired with a multislice multispin echo (MSME) sequence. Lower leg data were collected with the following parameters: in-plane resolution $(0.75\ \text{mm})^2$ with 7-mm slices (6–7 slices) separated by a 3.5-mm interslice gap, 16 echoes acquired with TEs evenly spaced from 20 to 320 milliseconds, and a TR of 3,000 milliseconds. Upper leg data were acquired with identical parameters, except in-plane resolution was $(1.0\ \text{mm})^2$.

Additional details of the MRI/MRS acquisitions, including reproducibility of the various measures, have been described previously.[9] Overall, reproducibility of FF and qT_2 values were excellent with average coefficients of variation of <5%.[9]

Functional testing

In addition to MRI/MRS data collection, all participants performed a timed 10-m walk/run functional test during each study visit.[19] For this test, participants performed 3 trials, and the fastest trial was used for analysis. If a participant was unable to complete the 10-m walk/run task within 45 seconds, or without assistance, the participant was considered to have lost the ability to perform the test. LOA age was defined here as the age at the first visit in which a participant was unable to perform the 10-m walk/run.

MRI/MRS analyses

MRS FFs were determined by spectral integration of fat (0.5–2.75 ppm) and ^1H_2O (4.3–5.10 ppm) signal regions from MRS acquisitions collected using a TE of 108 milliseconds and a TR of 3,000 milliseconds (figure 1) with correction for relaxation time effects, as previously described.[9]

Quantitative T_2 (qT_2) values were determined from voxel-wise fits performed with a single exponential function to MSME magnitude data, as previously described.[9] To improve consistency between participants and across time, predefined anatomic landmarks were used for region selection. For the lower leg, the initial slice in which the popliteus muscle was first visible and 2 additional contiguous slices were selected. In the upper leg, 3 contiguous slices were selected with the initial slice containing the biceps femoris short head. Using custom software, trained analyzers manually drew regions of interest on short-TE MSME images just within the borders of the lower and upper leg muscles, excluding fascia. The T_2 values of all voxels within the regions of interest drawn on the 3 analyzed slices were averaged to obtain mean muscle MRI qT_2, with values compiled for 5 lower leg muscles (SOL, medial gastrocnemius [MG], peroneus [PER], tibialis anterior [TA], and tibialis posterior [TP]) and 3 upper leg muscle (VL, biceps femoris long head [BFLH], and gracilis [GRA]).

Statistics and modeling

We used a nonlinear mixed-effect (NLME) model based on a normal cumulative distribution function (CDF; the integral of a Gauss function; see equation 1)[20] to capture the time dependence of MRI/MRS biomarker change:

$$E\left[Y_i(t)|\mu_i,\sigma_i\right] = A^*\int \exp\left\{-\left(t-\mu_i\right)^2\Big/2\sigma_i^2\right\}dt\Big/\left(\sigma_i\sqrt{2\pi}\right)+C \quad (1)$$

where MRS FF or MRI qT_2 value at age t is estimated by $E[Y_i(t)]$, μ_i represents the age at which the MRI biomarker change is half-maximum (and progression rate constant is greatest) for participant i, σ_i is the time constant of the MRI biomarker progression for participant i, A is the amplitude of biomarker total change, and C is the biomarker initial value. MRS FF measures from the VL and SOL were fitted using an NLME CDF model with C = 0.01 (i.e., FF = 0.01 at t = 0), A = 0.89, which was fixed for both muscles. Initial values for μ and σ were estimated and participant-level random effects for μ and σ were calculated for each muscle. MRI qT_2 measures from 8 muscles were modeled with equation 1 with A fixed at 59.2 milliseconds and C at 30.8 milliseconds for all muscles. All mixed-effect models were fitted using restricted maximum likelihood as implemented in the Nonlinear Mixed Effects Models library in R.[21] We constructed data summaries for MRS FF, qT_2, and population estimates from NLME modeling. All summaries are reported as mean (SD). For cross-sectional comparisons across 2 groups, we used Welch *t* tests. Linear regression was used to determine the association between MRS FF and MRI qT_2. A Cox proportional hazard model was used to estimate the added predictive value of μ, determined from MRS FF, for age at LOA; for these fits, we assumed that the μ values were linear on the log hazard scale.

Data availability

Anonymized data published within this article may be obtained by submitting a written request to the corresponding author.

Figure 1 Qualitative fat fraction changes in the leg muscles of a control and participant with DMD over 2 years

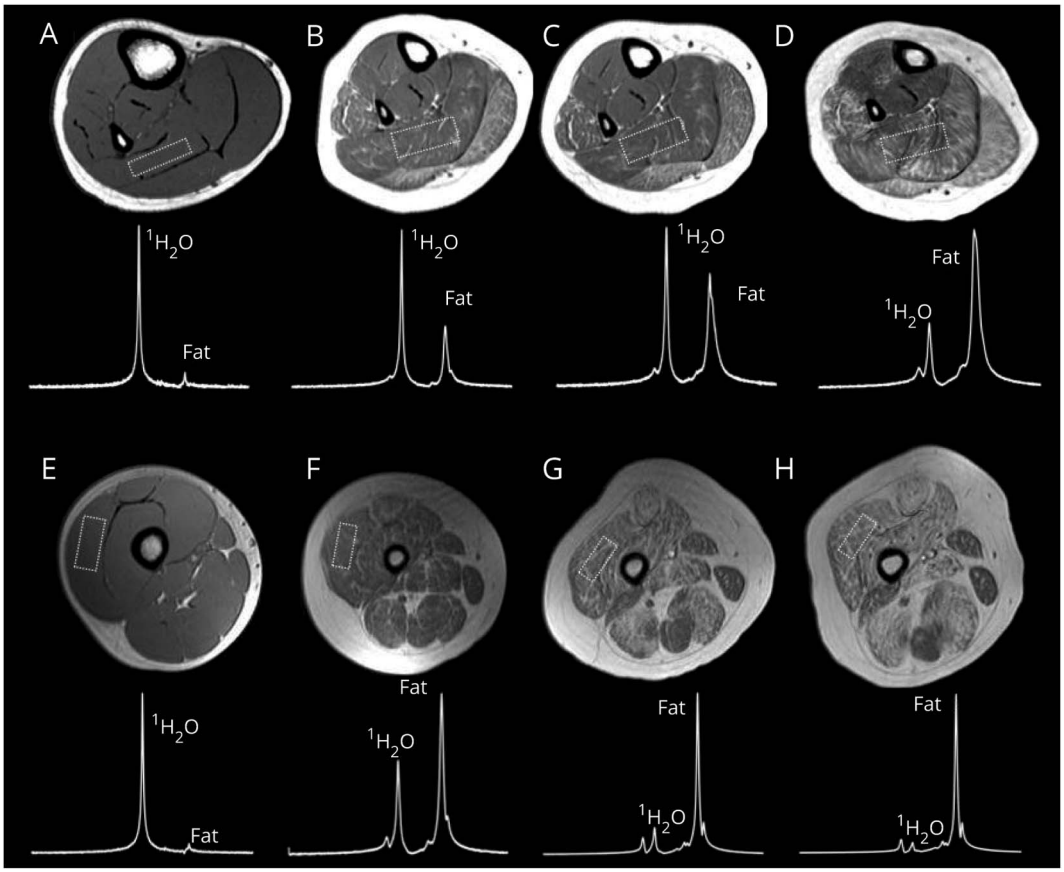

Axial T_1-weighted MRI of the (A–D) lower leg and (E–H) upper leg with the corresponding magnetic resonance (MR) spectroscopy (MRS) from the soleus and vastus lateralis muscles. MRI/MRS from a 9-year-old unaffected participant is shown in panels A and E. (B and F) Baseline MRI/MRS of a participant with DMD (age 5 years), (C and G) 1-year follow-up, and (D and H) 2-year follow-up. Fat deposits appear bright in these images, with greater contributions subcutaneously and intramuscularly in the participant with Duchenne muscular dystrophy (DMD) compared to an unaffected participant. The proton MR spectra are labeled to indicate water (^1H_2O) and principal fat peaks. As seen in the images, most muscle groups of the upper leg and lower leg show increased hyperintensity with age. In contrast, the tibialis anterior and posterior are relatively preserved across time.

All data-sharing requests will be reviewed by the ImagingDMD Executive Committee before approval.

Results

The baseline age range for 104 male patients with DMD included here was 4.2 to 16.9 years (median 8.6 years) and for 51 healthy male controls was 5.3 to 15.0 years (median 9.0 years). At study entry, 81 participants with DMD were being treated with corticosteroids and 23 participants with DMD were untreated. For the corticosteroid-treated group, the majority were using deflazacort (69%), followed by prednisone (26%), and prednisolone (5%). Of the 81 participants, 1 went off steroids within a year after enrollment, stayed off steroids for the remaining 5 years of the study duration, and was categorized as corticosteroid negative (Steroid−). Of the 23 participants with DMD who were not treated with corticosteroid at baseline, 10 transitioned to corticosteroid treatment after the baseline visit, remained on corticosteroids during their study participation, and hence were categorized as corticosteroid positive (Steroid+). We defined the remaining 13 participants as Steroid− because these individuals were not treated with corticosteroids during their study participation reported above. In summary, we had 90 Steroid+ and 14 Steroid− individuals with DMD in this study. There were no significant differences in the baseline demographic features between the 2 groups (Steroid+ vs Steroid− mean [SD]: age 8.9 [2.8] vs 8.5 [2.8] years, height 122.3 [12.5] vs 123.6 [13.8] cm, and weight 31.9 [13.2] vs 28.6 [11.3] kg). Furthermore, of 104 individuals with DMD, 28 participants experienced LOA during the study period.

At baseline, average FFs were significantly elevated ($p < 10^{-6}$) in individuals with DMD compared to healthy controls for both VL (0.187 [0.172] and 0.024 [0.015], respectively) and SOL (0.097 [0.072] and 0.024 [0.014], respectively) muscles with large effect sizes (Cohen d >1). Similarly, baseline qT_2 values were elevated in participants with DMD compared to controls for all muscles investigated ($p < 10^{-6}$; range: DMD 37.1–50.7 milliseconds, healthy controls 32.6–34.6 milliseconds, Cohen

d >1), with GRA, TA, and TP showing smaller differences than other muscles.

Figure 1 shows axial T_1-weighted images acquired from the lower and upper legs of 2 individuals, a healthy control (figure 1, A and E), and a 5-year-old patient with DMD (figure 1, B–D, F–H) collected at baseline and at annual 1-year follow-ups. A comparison between the images collected at annual follow-ups reveals a marked increase in signal hyperintensities in nearly all muscle groups, although greater increases are apparent in muscles proximal to the trunk. Modest or no increases are observed in TP, GRA, and TA. Visual inspection of the extent of hyperintensity on T_1-weighted MRI data is frequently used to evaluate muscle involvement in DMD using a qualitative scale.[22] In figure 1, ^{1}H MRS data, plotted below the imaging data, are labeled to indicate water proton and principal fat peaks. SOL and VL MRS FFs in DMD show marked increases with time.

In figure 2, A and B, MRS FF scatterplots illustrate the longitudinal behavior for SOL and VL, with symbols

Figure 2 Longitudinal magnetic resonance spectroscopy FF for VL and SOL muscles in DMD

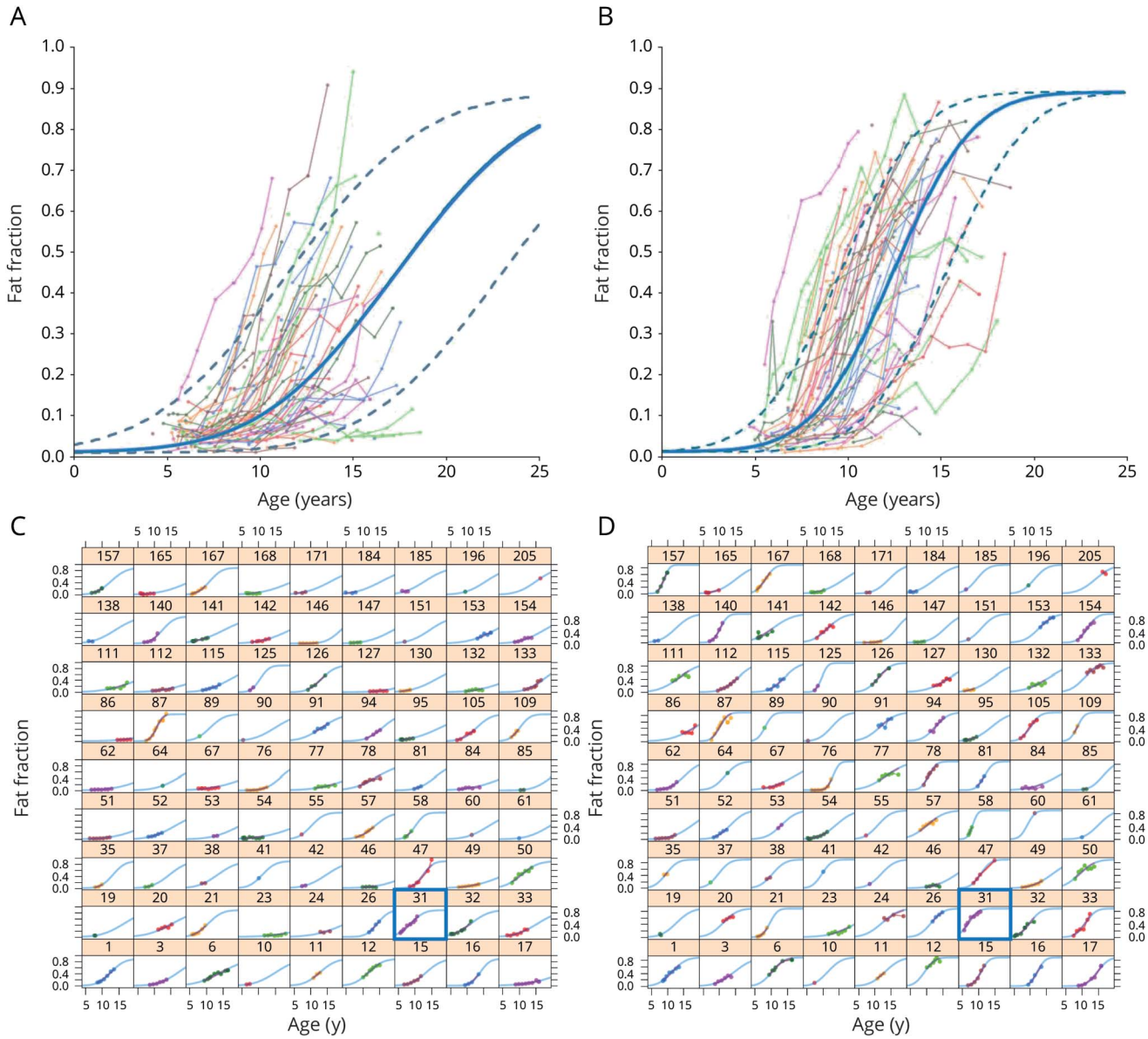

(A and B) Changes in soleus (SOL) and vastus lateralis (VL) fat fraction (FF) for individual participants. Each measurement is indicated by a filled circle, and tie lines connect individual participants. Substantial heterogeneity in FF progression can be observed between individuals. Solid blue curves in panels A and B represent population-average progression determined from nonlinear mixed effects modeling using equation 1 for SOL and VL, respectively, with A = 0.89 and C = 0.01. Dashed lines indicate 1 SD in average age at half-maximal muscle involvement (μ), calculated from values estimated for individuals (i.e., μ_i). (C and D) Breakout of the first 81 individual participants for each thumbnail plot. Filled circles represent FF values obtained at each visit, and the solid line shows the best model fit. Inspection of the individual fits demonstrates excellent fitting of individual disease progression for a wide range of progression rates. Data for the participant presented in figure 1 are indicated by the blue square.

indicating measurements from a single participant at a single time and tie lines relating measurements collected at different times. We observed a typical behavior, wherein the FF increased slowly early in the disease, accelerated in preadolescent years, progressed slowly in later stages of disease when there was little muscle left to be lost and replaced by fatty-fibrous infiltrate. This temporal behavior was well modeled with the CDF model (equation 1), indicating that the accumulation of fatty deposits in dystrophic muscles represents the temporal summation of the instantaneous fat accumulation rate function that shows a gaussian age dependence. Figure 2, C and D exhibit modeling at the individual level for the SOL and VL muscles, respectively. The filled symbols represent measured MRS FF values, and the smooth solid line shows best fits of equation 1 to the MRS FF data. As can be seen in these thumbnail plots, the CDF (equation 1) represented the observed data well, despite large differences in individual trajectories and the overall simplicity of the model function. NLME CDF modeling of MRS FF yielded significant effects of muscle type on estimates of both μ ($p < 10^{-6}$) and σ ($p < 10^{-6}$). VL muscle had lower average values for μ and σ compared to the SOL, with 4.8 years earlier age at half-maximal muscle involvement (μ) as well as 60% shorter σ reflecting more rapid progression in VL; note that σ is a time constant of disease progression and is the inverse of the disease progression rate constant. As illustrated in figure 2, we noticed a considerable heterogeneity in disease progression between individuals. The μ values from individuals ranged from 6.9 to 20.7 years for VL and from 8.7 to 33.1 years for SOL muscle; indicating disease progression rates differing by a factor of ≥3 between individuals.

Regression analysis revealed a strong linear association between MRI T_2 values and MRS FF in individuals with DMD ($R > 0.91$, $p < 10^{-6}$) as well as healthy controls ($R > 0.48$, $p < 0.001$), which is consistent with the findings of a previous report.[23] The relationship between FF and MRI qT_2 showed nearly identical slopes for the control and DMD groups, suggesting that the muscle fat content is a primary determinant of MRI qT_2.

Modeling for qT_2 biomarkers resulted in excellent fits for 8 leg muscles at both the individual level and population level. We observed findings for qT_2 modeling of SOL and VL muscles similar to those obtained from modeling FF (table 1). This analysis also yielded significant differences between upper and lower leg muscles for μ ($p < 10^{-6}$) and σ ($p < 10^{-6}$). On average, upper leg muscles demonstrated lower estimates of μ (by 5.5 years) and σ (by 3.5 years). Models showing qT_2 trajectories for individual muscles are shown in figure 3, and parameter values are summarized in table 1. The general trends displayed significant differences in trajectories between muscle groups, with the fastest progression found for BFLH and VL muscles; comparatively slower progression for SOL, MG, PER, and GRA; and the slowest progression for TA and TP muscles.

Table 1 Population-level NLME model parameters for MRS FF and MRI qT_2 in lower limb muscles

	Age at 50% change in measure, μ, estimate, y (SD)	Time constant of disease progression, σ, estimate, y (SD)
MRS FF		
VL (n = 100)	12.5 (2.9)	3.4 (1.1)
SOL (n = 102)	17.3 (5.8)	5.7 (2.7)
MRI qT_2		
BFLH (n = 99)	10.8 (2.6)	4.3 (1.4)
VL (n = 101)	11.8 (3.1)	5.3 (2.0)
GRA (n = 99)	17.0 (3.8)	7.5 (2.2)
MG (n = 103)	16.9 (4.6)	8.9 (2.9)
PER (n = 101)	16.1 (4.8)	8.1 (3.1)
SOL (n = 103)	15.6 (3.9)	7.8 (1.9)
TA (n = 102)	20.3 (5.8)	9.0 (3.4)
TP (n = 103)	24.6 (4.9)	12.3 (3.4)
MRI qT_2 average (SD)		
Upper leg	**13.2 (3.3)**	**5.9 (1.6)**
Lower leg	**18.7 (3.8)**	**9.2 (1.8)**

Abbreviations: BFLH = biceps femoris long head; FF = fat fraction; GRA = gracilis; MG = medial gastrocnemius; MRS = magnetic resonance spectroscopy; NLME = nonlinear mixed-effect; PER = peroneus; qT2 = quantitative T2; SOL = soleus; TA = tibialis anterior; TP = tibialis posterior; VL = vastus lateralis.
MRS FF global model parameters: A = 0.89, C = 0.01. MRI qT2 global model parameters: A = 59.2 milliseconds, C = 30.8 milliseconds.

We summarize the disease progression parameters extracted from modeling for the Steroid+ and Steroid− groups in table 2. The group average progression parameters indicated more rapid progression in the Steroid− group for most muscles with the average μ occurring 2.5 years earlier in Steroid− compared to Steroid+. In figure 4, the average MRS FF trajectories are plotted for VL and SOL muscles in individuals with DMD with and without corticosteroid treatment, with Steroid+ group trajectories shifted to greater age with average μ values delayed by 4.8 years for SOL. The more slowly progressing SOL muscle provided better sensitivity to detect the effect of corticosteroid treatment than the faster-progressing VL muscle (table 2). Corticosteroid treatment delayed progression time constants (σ) in all muscles, with increases ranging from 3% to 35%, indicating a muscle-dependent slowing of disease progression associated with corticosteroid treatment. Finally, similar to the effects of steroids on FF, the largest effects of corticosteroid treatment on qT_2 were observed for muscles with lower indices of disease progression, confirming the increased sensitivity of MR measures to detect a corticosteroid treatment effect in more slowly progressing leg muscles, primarily

Figure 3 Population-average trajectories for MRI qT_2 and annual ΔMRI qT_2 measures

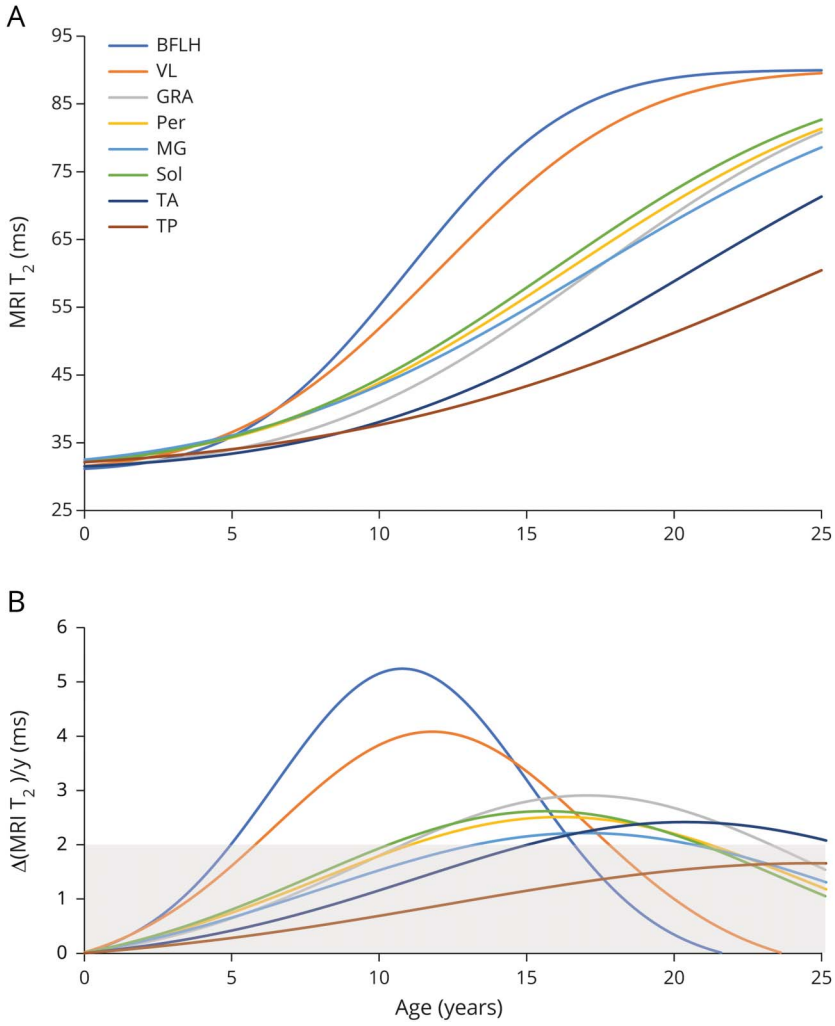

Population-average trajectories for (A) MRI quantitative T_2 (qT_2) and (B) annual ΔMRI qT_2 in muscles of the upper and lower leg. Biceps femoris long head (BFLH) and vastus lateralis (VL) muscles show the most rapid MRI qT_2 increase. The group average behavior of soleus (SOL), peroneus (PER), medial gastrocnemius (MG), and gracilis (GRA) muscles shows an intermediate increase in MRI qT_2 with time, and the tibialis anterior (TA) and tibialis posterior (TP) muscles have the slowest average MRI qT_2 progression. In panel B, the shaded area represents the 95% confidence interval of ΔqT_2 indicating no change for an individual participant. These muscles provide sensitivity to detect an annual qT_2 change in the individual from 5 to 25 years on the basis of 95% ΔqT_2 confidence interval of ≈2 milliseconds.

in the lower leg, compared to faster progressing leg muscles of the upper leg proximal to the trunk.

The VL and SOL are important muscles associated with ambulatory movements. The VL powers knee extension to support transition from a sitting to a standing position. The SOL is responsible for plantarflexion of the foot and provides the force to push off the ground during ambulation. Thus, the VL and SOL are promising candidates to serve as sentinel muscles associated with important clinical milestones such as LOA. Disease progression models using parameters from these muscles could provide predictive insight relevant to the clinical function.[24–26] In figure 5A, we have plotted the composite VL and SOL age at half-maximal involvement (μ) vs age at LOA, with regression (solid line) indicating a significant association ($p < 0.0001$) between these measures. To better quantify the value of VL μ as a surrogate for LOA, a Cox survival model was used. Results from the Cox proportional hazard model revealed significant associations of μ with LOA age for VL (LOA hazard ratio [HR] for 1-year decrement in μ 2.43, 95% confidence interval 1.77–3.35, $R^2 = 0.544$, $p < 10^{-6}$), SOL (HR 2.25, 95% confidence interval 1.65–3.05, $R^2 = 0.429$, $p < 10^{-7}$), and the composite measure of VL and SOL, VLSOL (HR 2.71, 95% confidence interval 1.92–3.81, $R^2 = 0.474$, $p < 10^{-7}$). To put this in context, for a 1-year decline in VL μ, the hazard of LOA increased by a factor of 2.43. In figure 5B, the estimated "survival" curves for time to LOA at 3 different VLSOL μ values (25th, 50th, and 75th percentiles of the estimated μ) are plotted on the basis of the Cox model fitting. It is clear that the LOA age increases for larger μ values.

Discussion

This study demonstrates the value of MR biomarkers in quantifying longitudinal changes in fat accumulation as a surrogate of DMD disease progression in lower and upper leg skeletal muscles. The principal new findings from this study are

Table 2 Population-level NLME model parameters for MRS FF and MRI qT_2 in lower extremity muscles with and without corticosteroid treatment

	Steroid+ age at 50% change in measure, μ, estimate, y (SD)	Steroid− age at 50% change in measure, μ, estimate, y (SD)	Steroid+ time constant of disease progression, σ, estimate, y (SD)	Steroid− time constant of disease progression, σ, estimate, y (SD)	Cohen *d*, differences in μ between Steroid+ and Steroid−
MRS FF (Steroid+, Steroid−)					
VL (n = 86, 14)	12.6 (2.8)	11.6 (3.2)	3.5 (1.1)	3.0 (1.4)	0.36
SOL (n = 88, 14)	17.9 (5.7)[c]	13.1 (3.9)	6.1 (2.7)[b]	3.4 (1.1)	0.84
MRI qT_2 (Steroid+, Steroid−)					
BFLH (n = 85, 14)	10.8 (2.6)	10.9 (2.7)	4.3 (1.4)	4.1 (1.2)	−0.02
VL (n = 87, 14)	11.9 (3.1)	11.1 (3.2)	5.4 (2.0)	4.1 (1.3)	0.27
GRA (n = 85, 14)	17.4 (3.9)[c]	14.3 (1.9)	7.7 (2.2)[b]	6.2 (1.7)	0.80
MG (n = 89, 14)	17.1 (4.7)[a]	14.6 (3.2)	8.9 (2.9)	8.6 (2.7)	0.53
PER (n = 87, 14)	16.6 (4.8)[b]	13.1 (3.9)	8.4 (3.1)[b]	6.0 (2.3)	0.74
SOL (n = 89, 14)	16.0 (3.9)[b]	13.1 (3.1)	7.9 (1.9)	6.8 (1.8)	0.73
TA (n = 88, 14)	20.3 (5.9)[b]	16.9 (4.5)	9.2 (3.4)[a]	7.3 (2.6)	0.66
TP (n = 89, 14)	25.2 (4.6)[a]	21.7 (5.6)	12.5 (3.3)	11.2 (3.9)	0.76
MRI qT_2 estimate (SD)					
Upper leg	**13.4 (3.5)**	**12.1 (1.9)**	**5.8 (1.7)**	**4.9 (1.1)**	**0.36**
Lower leg	**19.1 (3.9)**	**15.9 (3.6)**	**9.4 (1.8)**	**8.0 (2.0)**	**0.68**

Abbreviations: BFLH = biceps femoris long head; FF = fat fraction; GRA = gracilis; MG = medial gastrocnemius; MRS = magnetic resonance spectroscopy; NLME = nonlinear mixed-effect; PER = peroneus; qT_2 = quantitative T_2; SOL = soleus; TA = tibialis anterior; TP = tibialis posterior; VL = vastus lateralis.
MRS FF global model parameters: A = 0.89, C = 0.01. MRI qT_2 global model parameters: A = 59.2 milliseconds, C = 30.8 milliseconds.
Differences between Steroid+ and Steroid−: [a]$p \le 0.05$, [b]$p \le 0.01$, and [c]$p \le 0.001$.

the following: (1) increases of MRS FF and qT_2 with disease progression were well modeled at both the individual level and population level using a CDF that provides a sigmoidal age dependence; (2) disease progression time constants differed substantially between muscles; (3) corticosteroid treatment significantly delayed fat accumulation in most muscles, with the

Figure 4 Population estimates for FF trajectories for Steroid+ and Steroid− groups

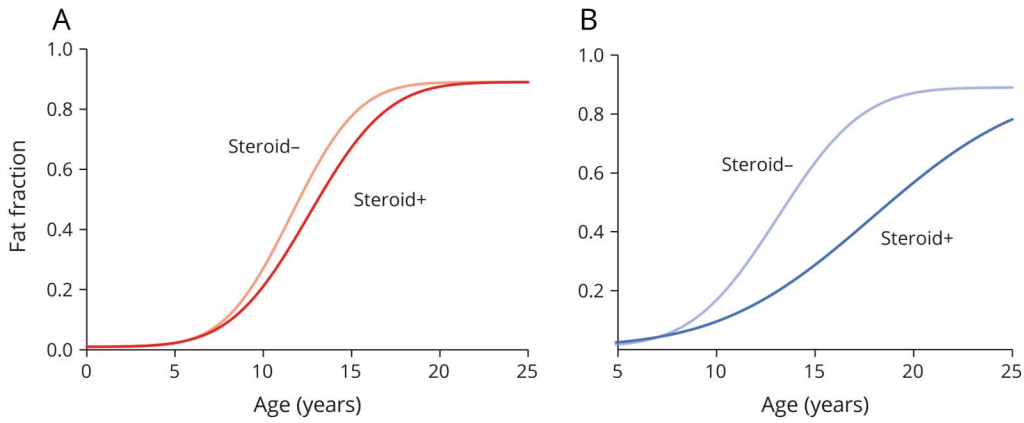

Population estimates for vastus lateralis (VL) and soleus (SOL) fat fraction (FF) trajectories with and without corticosteroid treatment. (A) VL and (B) SOL MRS FF age trajectories for participants with Duchenne muscular dystrophy who were treated with corticosteroid (solid lines, n = 86 for VL, n = 88 for SOL) and untreated (lighter lines, n = 14 for both VL and SOL). The population estimated age at half-maximum FF (μ) occurs 1.0 years earlier in VL and 4.8 years earlier in SOL in the corticosteroid-untreated compared to the corticosteroid-treated group. The disease progression time constant (σ) is 3.5 and 3.0 years for the VL corticosteroid-treated and untreated groups, respectively; σ is 6.0 and 3.9 years for the SOL untreated and corticosteroid-treated groups, respectively.

Figure 5 Relationship between age at LOA and μ for leg muscles

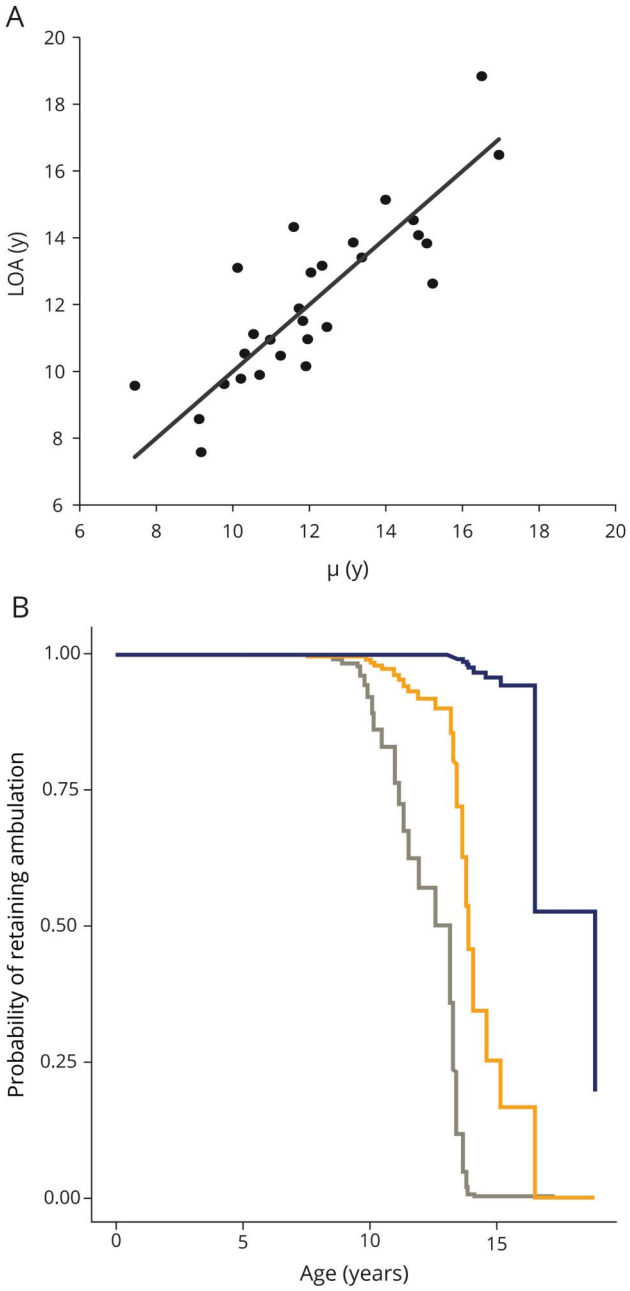

(A) Plot presenting the age at loss of ambulation (LOA) against the average age at half-maximal involvement (μ) for vastus lateralis (VL) and soleus (SOL) (μ = [μ(VL) + μ(SOL)]/2; VLSOL). Filled symbols represent individuals with Duchenne muscular dystrophy (n = 28), and the solid line represents the linear regression (LOA 1.0 μ), all with significant associations (r = 0.84; p < 0.0001) between LOA and μ. (B) Ambulation survival curves for VLSOL μ at 25 (gray), 50 (orange), and 75 (blue) percentile values demonstrating a substantially larger probability of retaining ambulation at older age with increased μ.

largest effect observed in more slowly progressing muscles; and (4) the age when VL and SOL FF reaches half-maximum (μ) is strongly associated with LOA in DMD.

In this study, we present detailed results from CDF NLME models to quantify DMD disease progression using MRS FF and MRI qT_2 measures, following up on our initial report.[20] Modeling MRI/MRS biomarkers in DMD is useful for several reasons. It reduces complex multidimensional datasets to simple, easy-to-understand metrics that can be tabulated and used more efficiently to summarize disease characteristics and progression at both individual and population levels. It also provides the opportunity to interpolate a sparsely sampled data time series such as those presented here. This is useful to obtain better time estimates of critical progression endpoints such as the time for an individual to reach a FF of 0.5 in the VL, which is a biomarker value relevant for LOA.[19] Modeling of MRI/MRS biomarkers in DMD also is useful for extrapolation, to estimate biomarker value for times outside of the sampling window (i.e., prognosis of disease progression). Finally, modeling large amounts of data, as presented here, allows better estimates of true disease progression, even in the presence of noise in measurements, and provides improved context for evaluating new therapeutic interventions.

NLME CDF modeling provides a simple and robust approach to quantify disease progression and captures the slow initial rise, fast midterm progression, and late-term tapering observed in muscle fat accumulation that characterizes the skeletal muscle progression in DMD. The CDF NLME modeling applied in this study provided excellent fits to MRS and MRI qT_2 data across all muscle groups. Notably, the observed sigmoidal behavior likely reflects the probabilistic nature of disease progression in DMD. A muscle cell has a finite number of cycles of injury/repair, due to inherent cellular repair processes, satellite cell depletion, and other mechanisms, before the cell is lost and replaced by a fatty-fibrous infiltrate.[27–30] We propose that early in the disease, the cumulative injury burden is low and reparative processes are functional, resulting in a low rate of muscle loss and fat replacement. The midterm disease progression is fast because a high fraction of muscle cells are at, or near, the injury/repair limit, and a large number of muscle cells remain that are available to be replaced. In the late term, while the probability of a muscle cell being at or near its injury/repair limit is high, there are few muscle cells remaining to be replaced, so the absolute magnitude of muscle loss and fat replacement at this stage is low. Of the 8 muscles investigated here, the VL and BFLH muscles progressed most rapidly, with VL MRS data indicating an average μ of 12.5 (2.9) years. The gluteus maximus muscle, although not studied here, is reported to progress even more rapidly than the VL. Using published cross-sectional MRS data of gluteus maximus and DMD age,[23] we can estimate an average μ of 9.1 (3.2) years, indicating that gluteus muscle reaches half-maximal involvement ≈3 years earlier than VL.

Corticosteroids are considered the standard of care in DMD due to their demonstrated positive impact on muscle strength, a multiyear delay in LOA, fewer respiratory and orthopedic complications, and decreased risk of death.[5–7,31,32] MR biomarkers have been shown to be sensitive to corticosteroid treatment, with both decreases in water T_2 and smaller changes in fat accumulation.[16] In this study, we found prolonged values of μ for muscles investigated in the Steroid+ group compared to

Steroid− group, with an average increase in μ of 2.5 years. This compares favorably with literature reports of prolonged ambulation by 1.9 years in deflazacort-treated patients treated with DMD compared to untreated patients.[5,7]

Our findings highlight that the natural history of individual muscle involvement and associated progression trajectory in DMD is highly variable. It is believed that the progression heterogeneity principally arises from differences in muscle load and stress, but other factors such as fiber-type composition might play a role.[33–35] Nevertheless, this heterogeneity provides an opportunity for an extended time frame to assess therapies. Consider that muscles such as VL and BFLH progress rapidly and on average will reach the point at which there is no muscle remaining to be rescued by disease-modifying agents earlier than muscles of the lower leg. More slowly progressing muscles such as SOL and MG are likely to remain in a stage when measuring their MRI/MRS change will provide a sensitive readout to therapeutic interventions, as observed in our own corticosteroid analysis. The higher sensitivity in the lower leg muscles likely reflects the fact that muscles at an early stage of involvement are more responsive to therapy. These observations emphasize the need and utility of careful characterization of the natural history of the disease using relevant biomarkers combined with appropriate time series modeling to provide confidence intervals of disease trajectory that can serve as a baseline for clinical trials. The ability of MRI/MRS to quantify the involvement of different muscles at varying stages of disease progression can prove extremely critical for determining the success of clinical studies. MR measurements, combined with proper modeling to capture DMD natural history, indicate that the time window of sensitivity for disease progression in the lower limb extends over 20 years. The noninvasive objective MR measures support a more complete picture of DMD disease burden, disease progression, and response to therapy.

Several limitations are associated with this study. First, because the project enrollment occurred on a rolling basis, the participants were studied for variable amounts of time. In addition, while participants were overall quite good at completing study requirements, some were unable to complete every measure at every study visit, which resulted in missing data. However, the modeling approach introduced in this study is a simple, reliable technique that is robust with respect to missing data; therefore, we are confident that these issues did not markedly affect our overall study findings. Next, although our results indicate marked increases in muscle disease progression rates for individuals off corticosteroids compared to those on corticosteroids, these comparisons were not based on controlled (randomized) groupings. Furthermore, we did not control the participants' corticosteroid treatment regimen or rigorously monitor compliance to steroid regimen during the study duration. Lastly, the LOA age was determined from yearly visit functional testing, and this approach has shortcomings with respect to timing accuracy. Therefore, in future studies, rigorous monitoring via monthly online parental surveys or phone calls would provide more accurate information on LOA.

This study presents a modeling approach to characterize MR biomarkers longitudinally and provides a comprehensive view of the natural history of skeletal muscle involvement in DMD. The CDF model that we used is simple and reliable and represents the data well across a wide range of progression characteristics. The modeling described here provides an efficient summary of complex temporal datasets with output parameters that are easy to understand, have biological significance, are relevant to clinical disease characteristics, are sensitive to treatment effects, and are available at individual and population levels. We applied the modeling to a large cohort of individuals with DMD and were successful in characterizing muscle progression rates that varied on the basis of proximity to trunk muscles, decreased with corticosteroid treatment, and associated strongly with LOA. Given the large number of individuals included in this study, the results likely are reflective of DMD progression in general. Although we applied this model to MR biomarkers, the technique is robust and could be extended to other measures of disease progression, including those in the clinical/functional domains.

Acknowledgment

The ImagingDMD study is supported by grant funding from the National Institute of Arthritis and Musculoskeletal and Skin Diseases and the National Institute of Neurological Disorders and Stroke of the NIH. The content is solely the responsibility of the authors and does not necessarily represent the official views of the NIH. The authors thank the participants and their families for their dedication and involvement in the study, and they are appreciative of the MR technologists and research staff who assisted in data collection and analysis.

Study funding

Funding provided by NIH National Institute of Arthritis and Musculoskeletal and Skin Diseases/National Institute of Neurological Disorders and Stroke R01AR056973, R01AR065943, 1U54AR052646 NIH S10OD021701, NIH S10OD018224, F30 DA033094, and R25 MH101076.

Disclosure

W.D. Rooney has received research support from the NIH, the Department of Defense, the Paul G. Allen Frontiers Group, the Conrad N. Hilton Foundation, the Race to Erase Foundation, and the Myelin Research Foundation. Y.A. Berlow has received research support from the NIH. W.T. Triplett, S.C. Forbes, and R.J. Willcocks report grants from the NIH. D.-J. Wang, I. Arpan, H. Arora, and C. Senesac report no relevant disclosures. D.J. Lott reports grants from NIH. G. Tennekoon reports funding from the NIH, Catabasis, Roche, PTC therapeutics, Sarepta, Italofarmaco. and Genetech. R. Finkel reports grants from ReveraGen, Roche, Catabasis, Capricor, and Italfarmaco. B.S. Russman reports research support from NIH and other support from Sarepta

Therapeutics. E.L. Finanger reports grants from NIH; personal fees and other from Sarepta Therapeutics and Catabasis; and other from PTC, Italfarmaco, Fibrogen, Summit Therapeutics, and Capricor. S. Chakraborty, E. O'Brien, B. Moloney, A. Barnard, H.L. Sweeney, and M.J. Daniels report no relevant disclosures. G.A. Walter reports grants from NIH. K. Vandenborne reports grants from NIH National Institute of Arthritis and Musculoskeletal and Skin Diseases/National Institute of Child Health and Human Development and Muscular Dystrophy Association; grants and other from Italfarmaco, Sarepta Therapeutics, Summit Therapeutics, Summit (Oxford) LTD, and Catabasis Pharmaceuticals; and other from Pfizer Inc, Idera Pharmaceuticals, Analysis Group, Eli Lilly and Co, and Critical Path Institute. Go to Neurology.org/N for full disclosures.

Publication history

Received by *Neurology* July 2, 2019. Accepted in final form October 17, 2019.

Appendix Authors

Name	Location	Contribution
William D. Rooney, PhD	Oregon Health & Science University, Portland	Design and conceptualized study; analyzed and interpreted the data; statistical analysis; drafted the manuscript for intellectual content, revised the manuscript for intellectual content
Yosef A. Berlow, MD, PhD	Oregon Health & Science University, Portland	Design and conceptualized study; analyzed the data; statistical analysis; interpreted the data; revised the manuscript for intellectual content
William T. Triplett, MS	University of Florida, Gainesville	Major role in the acquisition of data and data analysis; interpreted the data; revised the manuscript for intellectual content
Sean C. Forbes, PhD	University of Florida, Gainesville	Analyzed the data; interpreted the data; revised the manuscript for intellectual content
Rebecca J. Willcocks, PhD	University of Florida, Gainesville	Major role in the acquisition of data; analyzed the data; interpreted the data; revised the manuscript for intellectual content
Dah-Jyuu Wang, PhD	Children's Hospital of Philadelphia, PA	Major role in the acquisition of data, analyzed the data.
Ishu Arpan, PhD	Oregon Health & Science University, Portland	Analyzed the data; interpreted the data; revised the manuscript for intellectual content
Harneet Arora, PhD	University of Florida, Gainesville	Analyzed the data; interpreted the data; revised the manuscript

Appendix *(continued)*

Name	Location	Contribution
Claudia Senesac, PT, PhD	University of Florida, Gainesville	Major role in the acquisition of data, analyzed the data; interpreted the data; revised the manuscript for intellectual content
Donovan J. Lott, PT, PhD	University of Florida, Gainesville	Major role in the acquisition of data, analyzed the data; interpreted the data; revised the manuscript for intellectual content
Gihan Tennekoon, MBBS	Children's Hospital of Philadelphia, PA	Analyzed the data; interpreted the data; revised the manuscript for intellectual content
Richard Finkel, MD	Nemours Children's Hospital, Orlando, FL	Analyzed the data; interpreted the data; revised the manuscript for intellectual content
Barry S. Russman, MD	Oregon Health & Science University, and Shriners Hospital, Portland	Analyzed the data; interpreted the data; revised the manuscript for intellectual content
Erika L. Finanger, MD	Oregon Health & Science University, and Shriners Hospital, Portland	Analyzed the data; interpreted the data; revised the manuscript for intellectual content
Saptarshi Chakraborty, PhD	University of Florida, Gainesville	Analyzed the data; statistical analysis; interpreted the data
Elliott O'Brien, MS	Oregon Health & Science University, Portland	Analyzed the data; statistical analysis; interpreted the data
Brendan Moloney, MS	Oregon Health & Science University, Portland	Analyzed the data; interpreted the data
Alison Barnard, PT, PhD	University of Florida, Gainesville	Analyzed the data; interpreted the data; revised the manuscript for intellectual content
H. Lee Sweeney, PhD	University of Florida, Gainesville	Analyzed the data; interpreted the data; revised the manuscript for intellectual content
Michael J. Daniels, ScD	University of Florida, Gainesville	Design and conceptualized study; analyzed the data; statistical analysis; interpreted the data; revised the manuscript for intellectual content
Glenn A. Walter, PhD	University of Florida, Gainesville	Design and conceptualized study; analyzed the data; interpreted the data; revised the manuscript for intellectual content
Krista Vandenborne, PhD	University of Florida, Gainesville	Design and conceptualized study; analyzed the data; interpreted the data; revised the manuscript for intellectual content

References

1. Emery AE. The muscular dystrophies. Lancet 2002;359:687–695.
2. Hoffman EP, Brown RH Jr, Kunkel LM. Dystrophin: the protein product of the Duchenne muscular dystrophy locus. Cell 1987;51:919–928.
3. Straub V, Campbell KP. Muscular dystrophies and the dystrophin-glycoprotein complex. Curr Opin Neurol 1997;10:168–175.
4. Mah JK, Korngut L, Dykeman J, et al. A systematic review and meta-analysis on the epidemiology of Duchenne and Becker muscular dystrophy. Neuromuscul Disord 2014;24:482–491.
5. McDonald CM, Henricson EK, Abresch RT, et al. Long-term effects of glucocorticoids on function, quality of life, and survival in patients with Duchenne muscular dystrophy: a prospective cohort study. Lancet 2018;391:451–461.
6. Connolly AM, Schierbecker J, Renna R, Florence J. High dose weekly oral prednisone improves strength in boys with Duchenne muscular dystrophy. Neuromuscul Disord 2002;12:917–925.
7. Houde S, Filiatrault M, Fournier A, et al. Deflazacort use in Duchenne muscular dystrophy: an 8-year follow-up. Pediatr Neurol 2008;38:200–206.
8. Guiraud S, Davies KE. Pharmacological advances for treatment in Duchenne muscular dystrophy. Curr Opin Pharmacol 2017;34:36–48.
9. Forbes SC, Walter GA, Rooney WD, et al. Skeletal muscles of ambulant children with Duchenne muscular dystrophy: validation of multicenter study of evaluation with MR imaging and MR spectroscopy. Radiology 2013;269:198–207.
10. Straub V, Mercuri E, Aartsma-Rus A, et al. Report on the workshop: meaningful outcome measures for Duchenne muscular dystrophy, London, UK, 30-31 January 2017. Neuromuscul Disord 2018;28:690–701.
11. Straub V, Balabanov P, Bushby K, et al. Stakeholder cooperation to overcome challenges in orphan medicine development: the example of Duchenne muscular dystrophy. Lancet Neurol 2016;15:882–890.
12. Damon BM, Li K, Bryant ND. Magnetic resonance imaging of skeletal muscle disease. Handbook Clin Neurol 2016;136:827–842.
13. Forbes SC, Willcocks RJ, Rooney WD, et al. MRI quantifies neuromuscular disease progression. Lancet Neurol 2016;15:26–28.
14. Finanger EL, Russman B, Forbes SC, et al. Use of skeletal muscle MRI in diagnosis and monitoring disease progression in Duchenne muscular dystrophy. Phys Med Rehabil Clin N Am 2012;23:1–10, ix.
15. Triplett WT, Baligand C, Forbes SC, et al. Chemical shift-based MRI to measure fat fractions in dystrophic skeletal muscle. Magn Reson Med 2014;72:8–19.
16. Arpan I, Willcocks RJ, Forbes SC, et al. Examination of effects of corticosteroids on skeletal muscles of boys with DMD using MRI and MRS. Neurology 2014;83:974–980.
17. Pouwels PJ, Frahm J. Regional metabolite concentrations in human brain as determined by quantitative localized proton. MRS Magn Reson Med 1998;39:53–60.
18. Bruhn H, Frahm J, Gyngell ML, et al. Cerebral metabolism in man after acute stroke: new observations using localized proton NMR spectroscopy. Magn Reson Med 1989;9:126–131.
19. Barnard AM, Willcocks RJ, Finanger EL, et al. Skeletal muscle magnetic resonance biomarkers correlate with function and sentinel events in Duchenne muscular dystrophy. PLoS One 2018;13:e0194283.
20. Rooney WD, Berlow Y, Forbes SC, et al. Modeling Duchenne muscular dystrophy disease progression: a longitudinal multicenter MRI study. Proc Int Soc Magn Reson Med 2015;23:1227–27.
21. Pinheiro J, Bates D, DebRoy S, Sarkar D; R Core Team. NLME: linear and nonlinear mixed effects models [computer software and manual]. R Package Version 3 2014;1–117.
22. Mercuri E, Pichiecchio A, Counsell S, et al. A short protocol for muscle MRI in children with muscular dystrophies. Eur J Paediatr Neurol 2002;6:305–307.
23. Kim HK, Serai S, Lindquist D, et al. Quantitative skeletal muscle MRI: part 2, MR spectroscopy and T2 relaxation time mapping-comparison between boys with Duchenne muscular dystrophy and healthy boys. Am J Roentgenol 2015;205:W216–W223.
24. Willcocks RJ, Rooney WD, Triplett WT, et al. Multicenter prospective longitudinal study of magnetic resonance biomarkers in a large Duchenne muscular dystrophy cohort. Ann Neurol 2016;79:535–547.
25. Vuillerot C, Girardot F, Payan C, et al. Monitoring changes and predicting loss of ambulation in Duchenne muscular dystrophy with the Motor Function Measure. Dev Med Child Neurol 2010;52:60–65.
26. Fischmann A, Hafner P, Gloor M, et al. Quantitative MRI and loss of free ambulation in Duchenne muscular dystrophy. J Neurol 2013;260:969–974.
27. Morgan JE, Prola A, Mariot V, et al. Necroptosis mediates myofibre death in dystrophin-deficient mice. Nat Commun 2018;9:3655.
28. Rahimov F, Kunkel LM. Cellular and molecular mechanisms underlying muscular dystrophy. J Cell Biol 2013;201:499.
29. Jiang C, Wen Y, Kuroda K, et al. Notch signaling deficiency underlies age-dependent depletion of satellite cells in muscular dystrophy. Dis Models Mech 2014;7:997–1004.
30. Vila MC, Rayavarapu S, Hogarth MW, et al. Mitochondria mediate cell membrane repair and contribute to Duchenne muscular dystrophy. Cell Death Differ 2017;24:330–342.
31. Griggs RC, Miller JP, Greenberg CR, et al. Efficacy and safety of deflazacort vs prednisone and placebo for Duchenne muscular dystrophy. Neurology 2016;87:2123–2131.
32. Fenichel GM, Florence JM, Pestronk A, et al. Long-term benefit from prednisone therapy in Duchenne muscular dystrophy. Neurology 1991;41:1874–1877.
33. Gollnick PD, Sjödin B, Karlsson J, et al. Human soleus muscle: a comparison of fiber composition and enzyme activities with other leg muscles. Pflugers Arch 1974;348:247–255.
34. Webster C, Silberstein L, Hays AP, Blau HM. Fast muscle fibers are preferentially affected in Duchenne muscular dystrophy. Cell 1988;52:503–513.
35. Janghra N, Morgan JE, Sewry CA, et al. Correlation of utrophin levels with the dystrophin protein complex and muscle fibre regeneration in Duchenne and Becker muscular dystrophy muscle biopsies. PLoS One 2016;11:e0150818.